

MIT Open Access Articles

*The diabatic picture of electron transfer,
reaction barriers and molecular dynamics*

The MIT Faculty has made this article openly available. **Please share** how this access benefits you. Your story matters.

Citation: Van Voorhis, Troy et al. "The Diabatic Picture of Electron Transfer, Reaction Barriers, and Molecular Dynamics." Annual Review of Physical Chemistry 61.1 (2010): 149–170.

As Published: <http://dx.doi.org/10.1146/annurev.physchem.012809.103324>

Publisher: Annual Reviews

Persistent URL: <http://hdl.handle.net/1721.1/69649>

Version: Author's final manuscript: final author's manuscript post peer review, without publisher's formatting or copy editing

Terms of use: Creative Commons Attribution-Noncommercial-Share Alike 3.0



The diabatic picture of electron transfer, reaction barriers and molecular dynamics

Troy Van Voorhis¹, Tim Kowalczyk¹, Benjamin Kaduk¹,
Lee-Ping Wang¹, Chiao-Lun Cheng¹, and Qin Wu²

¹*Department of Chemistry,*

Massachusetts Institute of Technology

77 Massachusetts Ave.

Cambridge, MA 02139 USA

² *Center for Functional Nanomaterials,*

Brookhaven National Laboratory

Upton, NY 11973.

(Dated: July 15, 2009)

Abstract

Diabatic states have a long history in chemistry, beginning with early valence bond pictures of molecular bonding and stretching through the construction of model potential energy surfaces to the modern proliferation of methods for computing these elusive states. In this review we summarize the basic principles that define the diabatic basis and demonstrate how they can be applied in the specific context of constrained density functional theory. Using illustrative examples from electron transfer and chemical reactions, we show how the diabatic picture can be used to extract qualitative insight and quantitative predictions about energy landscapes. The review closes with a brief resumé of the challenges and prospects for the further application of diabatic states in chemistry.

Key Words: Reaction Dynamics, Nonadiabatic, Density Functional

Key Terms

- **Adiabatic State** An eigenstate of the Born-Oppenheimer electronic Hamiltonian.
- **Diabatic State** An electronic state that does not change character as a function of molecular geometry.
- **Diabatic Coupling** The matrix element of the electronic Hamiltonian between two different diabats: $V_{ij} = \langle \Psi_i | \hat{H}_{el} | \Psi_j \rangle$.
- **Density Functional Theory** A means of determining the ground state properties as a functional of the electron density.
- **On-the-Fly** Any technique wherein molecular energies and forces are calculated as needed rather than being inferred from precomputed values.

Important Acronyms

- **CDFT** Constrained Density Functional Theory
- **CDFT-CI** Constrained Density Functional Theory- Configuration Interaction
- **CT** Charge Transfer
- **DCT** Dielectric Continuum Theory
- **DFT** Density Functional Theory
- **ET** Electron Transfer
- **FAQ** Formanilide-Anthraquinone
- **MD** Molecular Dynamics
- **QM/MM** Quantum Mechanics/Molecular Mechanics
- **VB** Valence Bond

Summary Points

- Diabatic states provide an intuitive means of describing bonding by, for example, decomposing the wavefunction into ionic and covalent contributions.
- Diabats provide smooth potential energy surfaces that correspond to well-defined “product” and “reactant” channels.
- Mathematically, one cannot construct a set of strictly diabatic states out of a set of adiabats. As a result, there are many approximate prescriptions for diabats available to chemists.
- Constructive approaches facilitate the application of diabatic states in on-the-fly dynamics.
- CDFT provides a practical constructive route for obtaining approximate diabats in large molecular systems.
- Diabatic states provide a framework for obtaining quantitative predictions about ET dynamics and chemical reaction rates.

I. INTRODUCTION

Qualitatively, a diabatic electronic state is one that does not change its physical character as one moves along a reaction coordinate. This is in contrast to the adiabatic, or Born-Oppenheimer, electronic states which change constantly so as to remain eigenstates of the electronic Hamiltonian. A classic example of the interplay between diabatic and adiabatic pictures is given by sodium chloride dissociation (Figure 1). Here, the ground adiabatic state is thought of as arising from the avoided crossing between an ionic and a covalent state. The adiabatic state thus changes character - transforming from Na-Cl to $\text{Na}^+\text{-Cl}^-$ as the bond gets shorter - while the ionic and covalent configurations play the role of diabatic states.

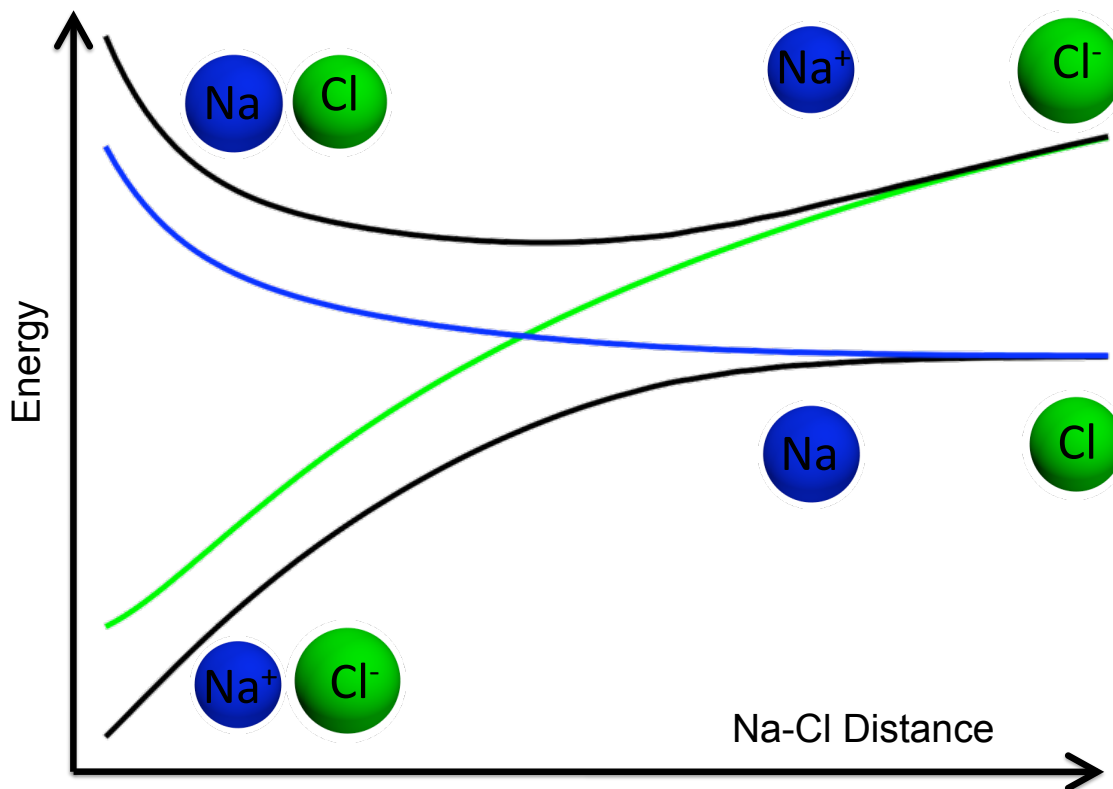


FIG. 1: NaCl dissociation in the diabatic and adiabatic representations. The ionic (green) and covalent (blue) diabatic states maintain the same character across the potential energy surface, while the adiabatic states (black) change.

Diabatic electronic states play a role in a variety of chemical phenomena but are, at the same time, under-appreciated by many chemists. For example, diabats are often used in the

construction of potential energy surfaces because they are smooth functions of the nuclear coordinates [1–3]. In spectroscopy, diabatic states are invoked to assign vibronic transitions and rationalize the rates of interstate transitions [4–6]. When describing electronically excited dynamics more generally, diabatic states are advantageous because they typically have a small derivative coupling, simplifying the the description of electronic transitions [7–11]. In scattering theory, diabatic states connect to clearly-defined product channels [12–14]. Finally, diabatic states play a qualitative role in our understanding of molecular bonding [15–17] (as illustrated by the NaCl example above), electron transfer [18, 19] and proton tunnelling [20–22]

This review article is intended as an introduction the basic concepts about how diabatic states are constructed and how they are used to describe chemical phenomena. After a summary of different definitions of diabatic states - and in particular why so many competing definitions exist - we focus on a particular definition based on constrained density functional theory (CDFT). We show how CDFT-derived diabatic states are computed in practice and discuss several illustrative chemical applications.

II. STRICT DIABATS CANNOT BE OBTAINED FROM ADIABATS

Of central importance to the study of diabatic electronic states is the idea of a strictly diabatic basis (SDB)[23]. By definition, for a set of strict diabats, $|\Phi_i\rangle$, the derivative coupling between any two states vanishes at every possible nuclear configuration, \mathbf{R} :

$$\mathbf{d}_{ij}(\mathbf{R}) \equiv \langle \Phi_i | \frac{\partial}{\partial \mathbf{R}} \Phi_j \rangle = 0 \quad \forall i, j, \mathbf{R} \quad (1)$$

This definition is in line with our qualitative idea that diabatic states do not change when the nuclei move (e.g. the derivative is zero). Given an arbitrary set of M adiabatic states, $|\Psi_i\rangle$ - say, a few important electronic states involved in a photochemical reaction - it would clearly be desirable to develop a formula for a set of M strictly diabatic states that span the same Hilbert space as the given adiabats. That is to say, one would like to have a set of orthonormal states that satisfy Eq. 1 and for which

$$|\Phi_i(\mathbf{R})\rangle = \sum_j A_{ij}(\mathbf{R}) |\Psi_j(\mathbf{R})\rangle \quad (2)$$

for some matrix \mathbf{A} . The matrix \mathbf{A} is called the adiabatic-to-diabatic transformation matrix, for obvious reasons[24, 25].

If states of this form could be obtained, they would clearly provide the most rigorous definition of diabatic states; one would simply need to specify the set of “interesting” adiabatic states, and then the corresponding diabatic states could be automatically determined. Unfortunately it is not generally possible to create an SDB from a given adiabatic basis[23] (See Sidebar).

Sidebar: Proof that one cannot create an SDB from a given adiabatic basis.

First write down the non-adiabatic coupling between the adiabatic states

$$\tau_{ij}(\mathbf{R}) \equiv \langle \Psi_i(\mathbf{R}) | \frac{\partial}{\partial \mathbf{R}} \Psi_j \rangle. \quad (3)$$

It is important to note that once the adiabatic states have been chosen, τ is fixed and cannot be changed. Now, write Eq. 1 in terms of τ and \mathbf{A} :

$$\begin{aligned} \langle \Phi_i | \frac{\partial}{\partial \mathbf{R}} \Phi_j \rangle &= \mathbf{A}^\dagger \tau \mathbf{A} + \mathbf{A}^\dagger \nabla \mathbf{A} = 0 \\ &\rightarrow \tau \mathbf{A} + \nabla \mathbf{A} = 0 \end{aligned} \quad (4)$$

Which can be considered the condition that determines the correct \mathbf{A} once the couplings are known[24, 25]. We now take the derivatives of Eq. 4 with respect to \mathbf{R} . After some manipulation, and exploiting the fact that mixed partial derivatives must be the same independent of the order in which they are taken, we obtain

$$\nabla \times \tau = \tau \times \tau. \quad (5)$$

This relationship is called the “curl condition” and it specifies a restriction that must be satisfied by τ if one hopes to construct an SDB out of the given set of adiabatic states. Unfortunately, this condition is not satisfied for the Born-Oppenheimer eigenstates of real molecules, except under rare circumstances[23, 26].

This result has a significant impact on how we approach diabatic states. One has the common situation where there is an ideal mathematical construction for diabatic states (SDBs) but no way of realizing this ideal in practice. Thus, if one wants diabatic states for a particular application, one must weaken the search criteria in one of two ways. One either looks for weakly diabatic states (i.e. ones that almost satisfy Eq. 5) that span a given adiabatic space, or one looks for strictly diabatic states that almost span the desired space. One expects that approximate diabats will be good descriptors of chemistry insofar

as they faithfully reproduce the strict diabats, and the approximations can be made better and better if one allows more and more states.

III. STRATEGIES FOR OBTAINING DIABATIC STATES

Given the results of the previous section, it is clear that we will need to make approximations to obtain practical diabatic states. As a rule, theoretical chemists enjoy making approximations, and thus it comes as no surprise that we have many, many subtly different ways of obtaining diabatic states for real systems. Broadly, these approaches can be broken down into two categories: techniques that try to deduce the best set of diabatic states from a given set of adiabats and those that attempt to construct diabatic states directly. The emphasis of this review is constructive methods, but in order to understand these techniques in context, we briefly summarize the most popular alternatives.

A. Deductive Strategies

- **Minimize the Coupling** If one cannot entirely remove the derivative couplings between diabatic states (Eq. 1) then one obvious strategy is to try to make the couplings as small as possible - typically in a local sense. The original proposal along these lines is due to Baer [24, 25] who proposed picking an arbitrary set of diabatic states at a reference point, \mathbf{R}_0 and then integrating Eq. 4 along a path (say, a reaction path) to obtain states that locally are strict diabats. This procedure turns out to be very computationally demanding, in part because it requires the derivative couplings at every point.
- **Slowly Varying States** Often one is looking for diabatic states that simply “do not change very much” from one point to another. The best established method in this family is the block diagonalization (BD) approach [27]. Here, one performs a unitary rotation in configuration space that block diagonalizes the electronic Hamiltonian, while leaving a target set of diabatic states as similar as possible to a reference set of states [28, 29]. It can be shown that this procedure minimizes the ℓ^2 norm of the derivative coupling ($|\mathbf{d}|^2 = \min$) in the vicinity of the reference point [30]. Other techniques in the same spirit include: enforcing configurational uniformity, so that

each diabatic wavefunction is predominantly constructed from a fixed set of electronic configurations [31, 32]; regularizing adiabatic states to remove the divergent portion of the coupling [33, 34]; and the fourfold way, which combines many of the positive features of the above methods [35, 36]. As a starting point, these techniques require a very accurate description adiabatic states and are thus typically used in conjunction with high-level CI calculations.

- **Eigenstates of a Physical Observable** By far the oldest form of diabatization is the Mulliken-Hush (MH) approach [37, 38] to electron transfer. Here, the approximate diabatic states are defined using purely spectroscopically observable information (transition energy, transition dipole μ_{12} and change in dipole $\Delta\mu$). This approach can be generalized to deal with multiple states in a way that only involves adiabatic quantities [39, 40] if one defines the diabatic states as the eigenstates of the dipole moment operator [39, 41]. Similarly, one can deal with multiple charge centers and/or excitation energy transfer by defining the diabatic states to be the maximally localized wavefunctions in real space [42, 43]. In each case, one realizes that the eigenstates of any fixed physical observable (such as the dipole or localization) will not change much as molecules rearrange, and thus form a transferable set of diabatic states. While computationally convenient, these techniques are typically only applied to electron- and energy-transfer problems.

B. Constructive Strategies

- **Valence Bond Theory** Although not widely publicized, Pauling’s idea of resonance structures within valence bond (VB) theory[44] provides a natural definition of diabatic states[45, 46]. For example, bonding in NaCl involves two resonance structures - $|\text{Na}^+ \text{Cl}^- \rangle$ and $|\text{Na} : \text{Cl} \rangle$ - which clearly have diabatic character from an electron transfer perspective. Allyl Radical has two structures - $|\text{CH}_2 = \text{CH} - \dot{\text{C}}\text{H}_2 \rangle$ and $|\dot{\text{C}}\text{H}_2 - \text{CH} = \text{CH}_2 \rangle$ - that place the double bond in a fixed location irrespective of which C-C bond is actually shorter. The VB-diabatic connection has been used to describe $\text{S}_{\text{N}}1$ reactions [47], proton-coupled electron transfer [48], and is the basis for the molecular orbital VB [49] and empirical VB [16, 17] methods. It is important to realize that, in order to get accurate diabatic states (i.e. in order to get diabatic

states that can faithfully reproduce the lowest several adiabats) it is often desirable to include more than the minimal number of diabatic states suggested by chemical intuition [50].

- **Density Constraints** In many cases, diabatic states can be clearly identified based on their density - ionic states like $|D^+ A^- \rangle$ will have excess electron density on one side of the molecule, while a covalent state like $|D^\uparrow A^\downarrow \rangle$ will have excess spin density on one side. Thus, suitable diabatic states can be obtained by optimizing the wavefunction subject to a constraint on the density. This concept is the basis of the frozen density functional method [51, 52] as well as the constrained DFT approach [53] detailed in the following section. Applying constraints is conceptually simpler than decomposing the wavefunction in terms of VB states, but can be computationally more challenging since it requires separate self-consistent calculations for each diabatic state.

IV. CONSTRAINED DENSITY FUNCTIONAL THEORY OF DIABATIC STATES

As a concrete example, we now focus on the specific choice of using density constraints to define diabatic states and outline the steps that must be taken to represent the electronic Hamiltonian, \mathbf{H}_{el} , in the constrained diabatic basis.

A. Obtaining diabatic states

By definition, we choose each diabatic state to be the lowest energy state of the system subject to a constraint on the density. For concreteness, it is good to have an example in mind, and we will use the $|D^+ A^- \rangle$ state of the formanilide-anthraquinone (FAAQ) molecule (Figure 2) as an illustration. This particular charge transfer excited state has been identified spectroscopically as having a very long lifetime ($>900 \mu s$) in DMSO solution. [54].

Step 1: Fragment Selection One must define a group of atoms whose charge/spin/electronic state one wants to constrain. Typically, this is done by chemical intuition, so that in the case of FAAQ, aniline (C_6H_6NH) is identified as the donor while anthraquinone ($COC_{14}H_7O_2$) is the acceptor.

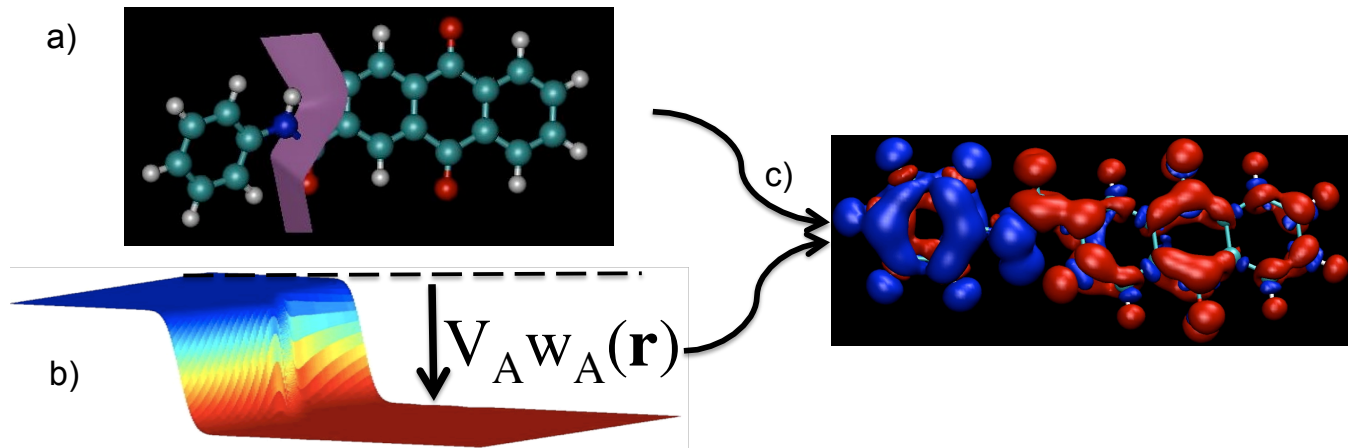


FIG. 2: Obtaining the D^+A^- state of FAAQ. a) One chooses which atoms belong to the acceptor. The atomic partition operator then divides space between the fragments, as illustrated by the dividing surface. b) Apply a constraint potential. Changing the Lagrange multiplier changes the depth of the potential and controls the number of charges on the acceptor. c) A ground state calculation in the presence of the optimal potential results in exactly one excess electron (red) on the acceptor and one excess hole (blue) on the donor.

Step 2: Defining the Constrained Observable In practice, there are any number of physical observables that one might constrain to create diabatic states: the dipole moment, the magnetic moment, the local spin state In the case of a charge transfer state, the obvious thing to constrain is the fragment charge [55]. But how do we define the fragment charge? Mulliken [56], Löwdin [57], Bader [58], Becke [59] and Hirshfeld [60] populations all provide useful but non-unique prescriptions for partitioning charge amongst different atoms within a molecule. For practical purposes, one must make an arbitrary choice at this stage and verify later that this choice does not materially affect the predictions. To this end, we might choose Becke’s partitioning wherein the charge on the acceptor is given by

$$N_A = \int w_A(\mathbf{r})(\rho^\alpha(\mathbf{r}) + \rho^\beta(\mathbf{r}))d\mathbf{r} \equiv \int w_A(\mathbf{r})\rho(\mathbf{r})d\mathbf{r} \quad (6)$$

where ρ is the electron density and w_A is the Becke weight operator that determines the charge on the acceptor. By design, $w_A(\mathbf{r})$ is nearly unity in regions of space near the acceptor, and nearly zero in regions of space near the donor[59] (See Figure 2). For the case of FAAQ, one clearly wants $N_A = -1.0$ so that the net charge on the acceptor

is -1. At the end of the calculations of Step 3 this choice will lead to the lowest energy state such that the the Becke partial charges of all the atoms in the acceptor sum to precisely -1.0.

Step 3 Constrained Minimization In order to obtain the lowest energy state subject to the constraint in Eq. 6, one introduces a Lagrange multiplier, V_A , and looks for the stationary point of

$$W[\rho, V_A] = E[\rho] + V_A \left(\int w_A(\mathbf{r})\rho(\mathbf{r})d\mathbf{r} - N_A \right) \quad (7)$$

where $E[\rho]$ is the electronic energy one is trying to minimize. One could apply this formalism to coupled cluster, reduced density matrix, or many body perturbation theory energy functions[61]. However, in Eq. 7 we specialize to the case of density functional theory both because it is relatively fast, and also because in principle it can give the exact energy of the system under any density constraint [53]. The stationary condition for V_A ($\frac{\partial W}{\partial V_A} = 0$) just enforces the constraint (Eq. 6). Meanwhile, in a Kohn-Sham (KS) framework, the stationary condition with respect to the density gives a Schrödinger equation for the KS orbitals:

$$\left(-\frac{1}{2}\nabla^2 + \int \frac{\rho(\mathbf{r}')}{|\mathbf{r} - \mathbf{r}'|}d\mathbf{r}' + v_{xc}(\mathbf{r}) + V_A w_A(\mathbf{r}) \right) \psi_i(\mathbf{r}) = \epsilon_i \psi_i(\mathbf{r}) \quad (8)$$

where v_{xc} is the exchange-correlation potential and ψ_i are the KS orbitals. Thus we see that the Lagrangian introduces an additional constraint potential, $V_A w_A(\mathbf{r})$, that controls the charge on the acceptor (see Figure 2). The optimal value of V_A is determined implicitly: the correct value of V_A modifies the KS equations in such a way that the resulting density ($\rho(\mathbf{r}) \equiv \sum_i |\psi_i(\mathbf{r})|^2$) satisfies Eq. 6. Because the implicit optimization is strictly a maximization, the simultaneous optimization of ρ and V_A can be accomplished in a similar amount of time to a standard ground state DFT calculation [61, 62]. Thus, in this constrained scheme, the diabatic states are obtained as adiabatic ground states of the system under an alternative potential.

This prescription can be simply generalized to deal with charge[55, 61, 62] and/or spin[63–66] constraints on an arbitrary number of fragments. We have implemented the above three step procedure into the NWChem[67] and Q-Chem[68] program packages. The result is that the user can specify not only the positions of the atoms, but also the the charge and spin on

any selected groups of atoms within the molecule. The fact that these are modified ground state calculations facilitates analytic force evaluation [55] as well as seamless integration into QM/MM and continuum electrostatic models of solvation.

Applying these steps to obtain both neutral ($|D A\rangle$) and charge transfer ($|D^+ A^-\rangle$) configurations for FAAQ using B3LYP[69] in the 6-31G* basis and COSMO[70] to describe solvation in DMSO, we find a relaxed charge transfer energy $\Delta G=2.31$ eV, which is in excellent agreement with the experimental measurement of 2.24 eV [54, 55]. Thus, constraints can be a quantitative tool for obtaining diabatic states in realistic molecules.

B. Computing the diabatic coupling

In the diabatic basis, the couplings, $V_{ij} = \langle \Psi_i | \hat{H} | \Psi_j \rangle$, play an analogous role to the derivative couplings in the adiabatic basis - both terms determine the rate of transitions between electronic states - but the diabatic couplings have the advantage of not requiring wavefunction derivatives. An accurate, simple expression for the diabatic coupling is particularly important because there are no quasi-classical formulae for V_{ij} . For example, the diabatic energies can quite often be estimated using classical expressions like the Rehm-Weller equation[71]. At the same level of theory, V_{ij} arises purely from quantum tunneling - the exponential tail of the donor wavefunction overlaps with the acceptor and vice versa - which has no classical counterpart. Thus, the diabatic coupling depends sensitively on the distance between the interacting fragments and their relative orientations, and a complete picture depends crucially on estimating it[72, 73].

V_{ij} also allows us to completely specify \mathbf{H}_{el} in the diabatic basis. For example, for two diabatic states

$$\mathbf{H}_{el} \equiv \begin{pmatrix} E_1 & V_{12} \\ V_{12} & E_2 \end{pmatrix}. \tag{9}$$

The energies, E_i are can be obtained directly from CDFT and only V_{12} is unknown. Note that, because they are eigenstates of different Hamiltonians, the pure constrained states are not orthogonal ($\langle \Psi_1 | \Psi_2 \rangle \equiv S \neq 0$). If one is interested in the diabatic coupling itself, physically one requires some orthogonal set of diabatic states - otherwise the overlap between the wavefunctions will be interpreted as a spurious coupling. A unique orthogonalization arises if all the diabatic states are specified by different averages of the same partition

operator, \hat{w} (e.g. if all the diabats have distinct charge/spin states for a single fragment within the molecule). In this case, one can look for the generalized eigenvectors, \mathbf{d} , of $\mathbf{W}\mathbf{d} = n\mathbf{S}\mathbf{d}$ and then $\mathbf{H} \rightarrow \mathbf{d}^\dagger \mathbf{H} \mathbf{d}$. These states are orthogonal and can be used to compute the coupling. To be clear, we will refer to the coupling in the non-orthogonal basis as V_{ij} while for the orthogonal coupling, we will use H_{ij} . In either case, the adiabatic states are defined by the generalized eigenequation

$$\mathbf{H}\mathbf{c} = \begin{pmatrix} E_1 & V_{12} \\ V_{12} & E_2 \end{pmatrix} \begin{pmatrix} c_1 \\ c_2 \end{pmatrix} = \epsilon \begin{pmatrix} 1 & S \\ S & 1 \end{pmatrix} \begin{pmatrix} c_1 \\ c_2 \end{pmatrix} \equiv \epsilon \mathbf{S}\mathbf{c}. \quad (10)$$

In the present context, the challenge in computing $\langle \Psi_i | \hat{H} | \Psi_j \rangle$ using constrained DFT is that DFT only gives us access to the energy and density of each diabatic state - the wavefunction is never constructed [74]. Hence, we will need to make an approximation to evaluate V_{ij} . Toward this end, we note that for constrained diabatic states, each diabat (i) is an eigenstate of the Hamiltonian in its own alternative potential ($V_i \hat{w}_i$)

$$\hat{H} + V_i \hat{w}_i | \Psi_i \rangle \equiv \hat{H}_i | \Psi_i \rangle = F_i | \Psi_i \rangle \equiv (E_i + V_i N_i) | \Psi_i \rangle \quad \forall i \quad (11)$$

where E_i , V_i and N_i are the diabatic energy, associated Lagrange multiplier and specified constraint value, respectively, for the i^{th} diabat - all of which are provided directly by constrained DFT. This allows us to re-write the diabatic coupling in the suggestive form [75]

$$\langle \Psi_i | \hat{H} | \Psi_j \rangle = \frac{1}{2} \langle \Psi_i | \hat{H}_i - V_i \hat{w}_i + \hat{H}_j - V_j \hat{w}_j | \Psi_j \rangle = \frac{F_i + F_j}{2} \langle \Psi_i | \Psi_j \rangle - \frac{1}{2} \langle \Psi_i | V_i \hat{w}_i + V_j \hat{w}_j | \Psi_j \rangle \quad (12)$$

Thus, the many-body matrix elements of \hat{H} in the diabatic basis can be reduced to a combination of zero-body (i.e. wavefunction overlap) and one-body (constraint potential) matrix elements. Eq. 12 contains the physical insight that the coupling between diabats only depends on the overlap between them (first term) and the potential required to create them (second term).

At this stage, we make an approximation and use the KS determinants $|\Phi_i\rangle$ in place of the exact diabatic states $|\Psi_i\rangle$ in Eq. 12. This is certainly an approximation, but it is one that works surprisingly well in practice[75]. For example, if we examine hole transfer in the mixed valence system Zn_2^+ as a function of the Zn-Zn distance, we expect that the tunneling matrix element will decay exponentially[40]. Using B3LYP and a large basis [40, 76] one

finds values for H_{ij} that differ by $<150 \text{ cm}^{-1}$ from the corresponding BD predictions for $5\text{\AA} < R < 9\text{\AA}$ [40]. The differences can largely be attributed to the underlying electronic structure - the BD used CASSCF, whereas the CDF'T results use B3LYP. Thus the present prescription for H_{ij} appears to be adequate for the coupling of well-separated fragments.

V. APPLICATIONS

A. Electron Transfer

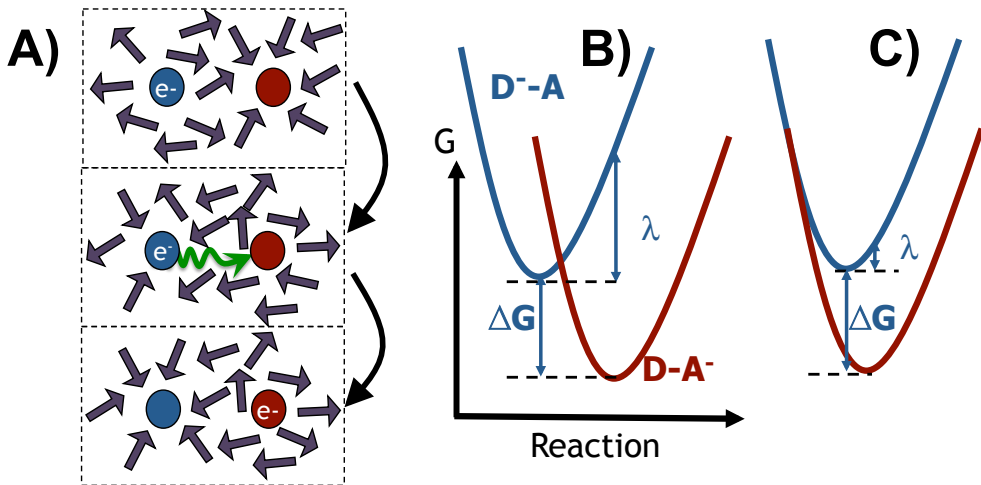


FIG. 3: A) In solution, the electron transfer reaction coordinate is dominated by solvent reorganization. The free energy landscape can be characterized by the driving force (ΔG), measuring the energy released, and reorganization energy (λ), measuring the structural relaxation energy. B) If $\Delta G < \lambda$ the reaction is in the normal regime and the rate increases with ΔG , but C) if $\Delta G > \lambda$ the reaction is inverted and the rate decreases with increasing ΔG

Diabatic states play a critical role in the theory of electron transfer (ET) (See Figure 3) [19, 77]. One first posits the existence of reactant and product diabatic states where the electron is localized on the donor and acceptor, respectively. Reactions are then typically characterized by the thermodynamic driving force, ΔG , and the reorganization energy, λ , of the diabatic free energy surfaces. The latter quantity measures the “stiffness” of the molecular framework - which can often be inferred from the Stokes shift of the charge transfer absorption/emission bands [78]. If we assume that the free energy surfaces are perfect parabolas with the same curvature (equivalent to assuming the system responds

linearly), it is easy to work out that the activation energy for ET is $\Delta G^\ddagger = (\Delta G + \lambda)^2/4\lambda$ leading to a rate[79, 80]:

$$k_{ET} \propto |H_{DA}|^2 \frac{1}{\sqrt{4\pi\lambda kT}} e^{-\Delta G^\ddagger/kT} = |H_{DA}|^2 \frac{1}{\sqrt{4\pi\lambda kT}} e^{-\frac{(\Delta G + \lambda)^2}{4\lambda kT}}. \quad (13)$$

There are many generalizations of this simple formula that account for anharmonic free energy surfaces [81], adiabatic electron transfer [82] and quantum nuclear effects [83]. In the present article, we will be interested in a more basic question: given that Eq. 13 or one of its generalizations is appropriate for a given problem, how can one compute accurate diabatic ET states and extract from those states parameters like ΔG and λ ? That is to say, how do we translate the cartoon (Figure 3) into a calculation?

The use of constrained DFT to answer this question traces its roots back to Wesolowski and Warshel’s [51, 52] idea of using a frozen density to describe the charge distribution of each diabatic state. More recent work has used constrained DFT (or the related concept of penalty function DFT) to define the diabatic potential surface, which can then be explored to estimate ΔG and λ [55, 84]. To do this, we need to define the reaction coordinate. Figure 3A) illustrates the physical picture[85]: when the electron is on the donor(acceptor), the solvent orients to stabilize the electron on the donor (acceptor). The transition state involves a fluctuation of the solvent that untraps the electron and initiates transfer. This picture leads to several reasonable choices for the reaction coordinate: one can choose the equilibrium solvent polarization [85], the fractional degree of electron transfer ($D^{-1+q} A^{-q}$) [86], or the energy gap ($\Delta E = E_D - E_A$) [87] between reactants and products. In what follows, we will show preference toward the last definition, which has certain formal advantages [88].

Once the diabatic states have been defined, the key remaining decision for condensed phase ET is how one treats the solvent. In some sense, the presence of solvent actually validates the use of diabatic states, so some care needs to be taken here [89]. Broadly speaking, there are two paths to choose from: implicit models - where the solvent is replaced by a fictitious continuous medium - and explicit models - where many discrete solvent molecules are included in the simulation. In order to compute $\Delta G \equiv G_D^{eq} - G_A^{eq}$ and $\lambda \equiv G_A^{neq} - G_A^{eq}$. one requires three free energies: 1) G_D^{eq} - the equilibrium free energy of the donor state 2) G_A^{eq} - the equilibrium free energy of the acceptor state 3) G_A^{neq} - the free energy of the acceptor state in the ensemble of nuclear configurations (q_D) most favorable for the donor. The first two are obviously equilibrium properties, while G_A^{neq} requires a non-

equilibrium Frank-Condon approximation, wherein the nuclear positions are all fixed by the donor ensemble but the solute and solvent electrons are relaxed in the acceptor electronic state. We now briefly review how these free energies are computed in the presence of solvent.

1. *Implicit Solvent*

At a basic level, an implicit solvent model has two steps. First, one carves out a spatial cavity around the solute molecule(s). Second, one fills the space outside the cavity with a dielectric medium, which represents the solvent. Because a dielectric can respond to the molecular charge distribution inside the cavity, this prescription provides a crude approximation to the electrostatic interaction between solvent and solute. This dielectric continuum theory (DCT) has a long history within chemistry. In the days before computers, these models were popular primarily because they can provide simple, analytic formulae for the solvation energy of a molecule [82, 85, 90, 91]. As time has progressed, these models have become more and more sophisticated [92–95] so that modern DCT is considered a computational and essentially predictive model of both chemical and biological phenomena.

The advantage of using DCT in describing electron transfer is that it vastly reduces the number of degrees of freedom one must explore because the solvent molecules have been “integrated out”. Thus, one can compute equilibrium free energies like G_D^{eq} or G_A^{eq} directly by optimizing the the geometry of FAAQ with the electron constrained to be on the donor (D A) or acceptor (D⁺ A⁻) in the presence of the solvent dielectric. Since analytic gradients of the energy are readily calculated in constrained DFT, geometry optimizations of this type are straightforward and the positions of individual solvent molecules need never be considered [55]. Applying this prescription to FAAQ using B3LYP/6-31G*/COSMO calculations, we obtain $\Delta G = 2.31$ eV which, as noted above, is in excellent agreement with experiment ($\Delta G = 2.24$ eV). Similarly, for a ferrocene adduct of FAAQ (Fc-FAAQ) the computed ΔG goes down to 1.02 eV, still in excellent agreement with the experiment at 1.16 eV[54, 55].

In order to compute λ one requires G_A^{neq} , which is somewhat tricky to obtain in a continuum model. The difficulty is that, because we have integrated out all the solvent degrees of freedom, it is challenging to freeze the solvent nuclei while allowing the solvent electrons to relax. To overcome this, one assumes the solvent dielectric has a “fast” component ($\epsilon_\infty \approx n_{opt}^2$) arising from electronic polarization, and a total dielectric (ϵ_0) which

captures electronic+nuclear response. Each dielectric, $\epsilon = \epsilon_\infty, \epsilon_0$, interacts with the solute through a reaction field V_0 [92]

$$V_0 = -g(\epsilon_0)V_{solute} \equiv -\frac{\epsilon_0 - 1}{\epsilon_0}V_{solute} \quad (14)$$

where V_{solute} is the potential of the solute on the boundary (B) of the cavity[96]. From Eq. 14, we identify the “slow” field as

$$V_{slow} = (g(\epsilon_0) - g(\epsilon_\infty))V_{solute} \quad (15)$$

which simply interprets the slow part as the difference between the total and fast components. In order to compute G_A^{neq} , then, one first performs a calculation with the electron on the donor and obtains V_{slow} . One then performs a calculation at the same geometry with the electron on the acceptor and two fields: 1) A static field of V_{slow} and 2) A polarizable continuum with dielectric ϵ_∞ . These two fields reflect, respectively, the nuclear part of the solvent (which is frozen) and the electronic part (which responds). Finally, denoting the acceptor electron density and potential by ρ^A, V^A and similarly for the donor [97]

$$G_A^{neq} \equiv E[\rho^A] - \frac{1}{2}g(\epsilon_\infty) \int_B V^A(\mathbf{r})\rho^A(\mathbf{r})d\mathbf{r} - \int_B V_{slow}(\mathbf{r})\rho^A(\mathbf{r})d\mathbf{r} + \frac{1}{2} \int_B V_{slow}(\mathbf{r})\rho^D(\mathbf{r})d\mathbf{r}. \quad (16)$$

If we apply this prescription to FAAQ and Fc-FAAQ using B3LYP/6-31G*/COSMO calculations, we obtain $\lambda_D = \lambda_A = .6$ eV for FAAQ and $\lambda_D = \lambda_A = .8$ eV for Fc-FAAQ. These results are qualitatively consistent with the experimental observation that FAAQ is in the inverted regime, so that $\lambda \ll \Delta G$, while Fc-FAAQ undergoes rapid charge recombination, which implies $\Delta G \approx \lambda$ [54]. However, the results are quantitatively incorrect: one infers a value of $\lambda \approx 1.45$ eV from the experimental kinetics, which is much higher than either DCT prediction. The disagreement likely has to do with the fact that modern DCT is heavily parametrized toward equilibrium properties, with relatively less attention paid to the type of non-equilibrium solvation involved here. To obtain a more consistent results away from equilibrium, one turns to explicit models.

2. *Explicit Solvent*

Explicit solvent models offer manifold advantages over implicit models: one can directly probe reaction dynamics; one obtains information about the entire free energy surface; and

one can obtain parameter free *ab initio* predictions of free energies. The downside is that explicit solvent calculations are 1,000 to 1,000,000 times as expensive as their implicit counterparts and the rapidity with which results can be obtained is thus somewhat hindered. The seminal papers in the field use classical force fields to describe the diabatic potential energy surfaces, in which case the calculations are much faster. These investigations established rate expressions [98–100], mapped out the free energy surfaces [87, 101], validated the reaction coordinate [102, 103] and predicted qualitative reaction dynamics [86, 104].

More recently, advances in computer speed have opened the possibility of exploring the diabatic ET energy landscape in explicit solvent using DFT. [63, 66, 84, 105–110]. The general prescription for these simulations is illustrated in Figure 4, again for the example of FAAQ in DMSO. First, one performs several long molecular dynamics (MD) trajectories for each diabatic state in the presence of solvent in order to properly sample the energy landscape. These simulations would be virtually impossible with a deductive prescription for the diabatic states - which would require derivatives of excited state wavefunctions and/or the identification of a reference structure. For constrained DFT, one merely requires ground state energy derivatives to perform the relevant on-the-fly Born-Oppenheimer-like dynamics [55]. For example, in the simulations in Figure 4, the solvent was modeled by a polarizable force field and the diabatic states of FAAQ were determined by constrained B3LYP/3-21G. The technical details of the computations can be found elsewhere[110]. However, note that a traditional fixed-charge model of the solvent (as opposed to the polarizable approach used here) would result in severe overestimation of the reorganization energy [110, 111] essentially neglecting all the “fast” component of the dielectric response.

Once the MD simulations are complete one harvests a large number of independent snapshots from the trajectories and computes the energy of both diabatic charge states at every snapshot. By performing this procedure for the neutral and CT trajectories of FAAQ, one obtains the two energy gap distributions displayed in Figure 4c) and 4d), respectively. Finally, one can obtain the free energy surfaces from

$$G_X(\Delta E) \equiv -kT \ln P_X(\Delta E) \quad X = CT \text{ or } N. \quad (17)$$

In Figure 4e) we present a simplified fit of this type wherein G_N and G_{CT} are assumed parabolic with the same curvature. Under these circumstances, G_N and G_{CT} are determined entirely by ΔG and λ , facilitating a direct comparison to the Marcus picture. We find that

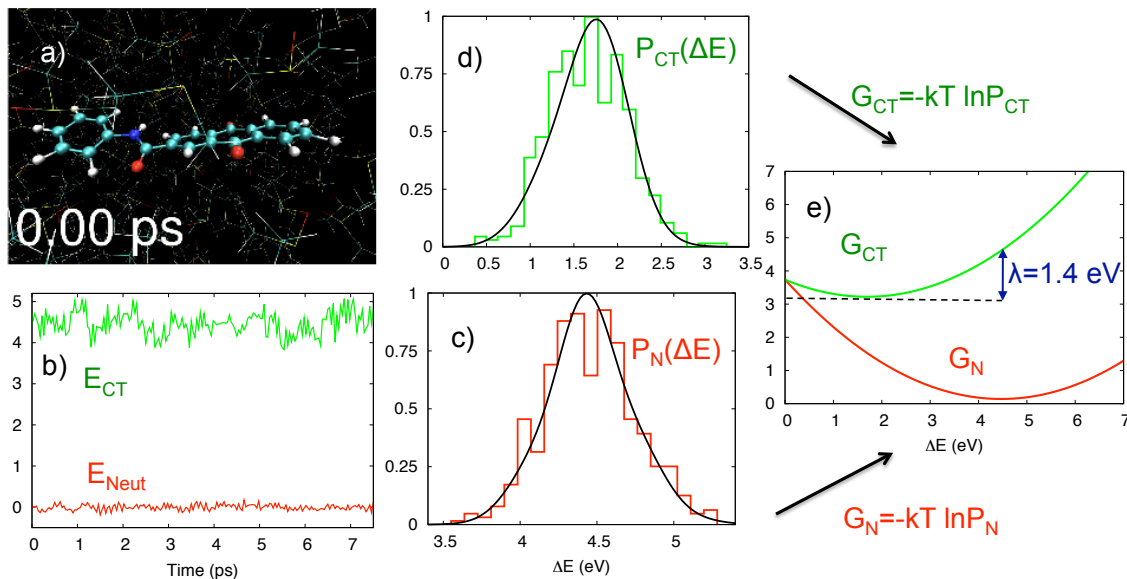


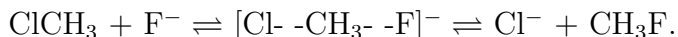
FIG. 4: Sampling the ET energy landscape with explicit solvent. a) One first computes several long MD trajectories, with the solute in either the neutral (pictured) or CT state. A movie of one such trajectory is available in the supporting material. b) One monitors the energy of each diabats as a function of time and collects statistics on the energy gap ($\Delta E = E_{CT} - E_N$) from the neutral (c) and CT (d) trajectories. Here, the histograms show accumulated data, while the lines are a maximum likelihood fit. e) Finally, the free energy, G of each state is computed from the log of the probability computed in parts c) and d). All energies are in eV.

$\Delta G \approx 3.1$ eV for FAAQ, which is too high compared to experiment primarily because a small basis (3-21G) has been used for the electronic structure. It is anticipated that similar simulations in a 6-31G* basis would be more in line with experiment. Meanwhile, we obtain $\lambda \approx 1.4$ eV - which is in excellent agreement with experiment ($\lambda \approx 1.45$ eV). A larger basis would likely have little effect on λ because it primarily reflects the geometry of the system, which should be less sensitive to the electronic basis. It thus appears that implicit models offer a fast and reasonably accurate means of predicting equilibrium properties of the diabats (like ΔG), but that they should be supplemented by explicit solvent when out-of-equilibrium behavior (like reorganization) is of interest.

B. Chemical Reactions

The diabatic picture employed for electron transfer can also be applied to more general reactions. Instead of “donor” and “acceptor” electronic states, one posits “product” and “reactant” diabats that exist at all points along the reaction coordinate. This diabatic framework is the basis of empirical VB theory [16, 17] and has been used to analyze S_N1 [47] and S_N2 [112] reactions, as well as proton transfer [21]. Once the diabatic states are defined, one is typically interested in computing the corresponding adiabatic energies by solving the generalized eigenvalue problem in Eq. 10 at every nuclear configuration. One can then predict activation energies and transition pathways as well as decompose the transition state electronic structure into “reactant” and “product” contributions. In this section, we will briefly touch on some recent work in our group that attempts a systematic description of a wide range of reactions using the reactant/product division within constrained DFT.

The first task, of course, is to construct the reactant and product diabatic states. The task at hand is more challenging than for ET because in a typical chemical reaction, atoms are exchanged between the reactant and product molecules. Thus, while one can reasonably bin atoms as part of the “donor” or the “acceptor” fragment in an ET reaction, the same will not generally be true in, say, an S_N2 reaction. We have recently shown this obstacle can be overcome if one assumes that the reactant state density should resemble the superposition of the densities of the reactants[110, 113]. To be concrete, suppose one is interested in a nucleophilic substitution reaction:



Clearly, the reactant state should formally have zero charge ($q = 0$) and no net spin ($S = 0$) on the ClCH_3 group and [$q = -1, S = 1/2$] on F^- . Likewise, the product state should have $\text{Cl}(q = -1, S = 1/2)$ and $\text{CH}_3\text{F}(q = 0, S = 0)$. Now, we realize that the formal charges and spins will be precise when the fragments are well-separated, but these values are not expected to be accurate constraints at the transition state, where the fragments overlap significantly.

To obtain the correct constraint values for the reactant state (an equivalent procedure is followed for the product) one generates a promolecule density $\tilde{\rho}_R$ by superimposing the densities of ClCH_3 and F^- , calculated separately with their formal charges and spins and at

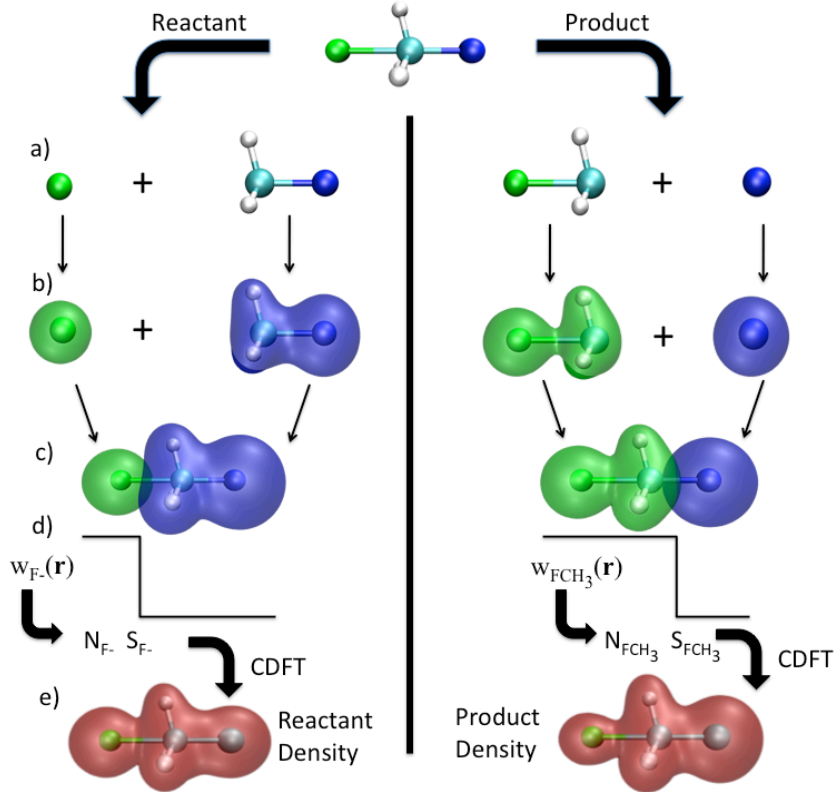


FIG. 5: Constructing reactant and product diabatic states for $F^- + CH_3Cl \leftrightarrow FCH_3 + Cl^-$. a) The atoms are divided according to the reactants and products b) DFT calculations are performed on the isolated fragments c) The fragment densities are added together d) The apparent charge (N) and spin (S) for each fragment are determined by integrating the population weight function $w_i(\mathbf{r})$ against the summed densities e) Constrained DFT calculations are performed with the computed $N+S$ constraints to arrive at the reactant and product diabats.

the same level of theory as the final calculation, i.e.

$$\tilde{\rho}_R^\sigma(\mathbf{r}) = \rho_{ClCH_3}^\sigma(\mathbf{r}) + \rho_{F^-}^\sigma(\mathbf{r}) \quad (\sigma = \alpha, \beta). \quad (18)$$

Note that the $ClCH_3$ fragment internal geometry is identical to the geometry of said fragment within the full calculation. The reactant charge and spin constraints of a given fragment ($X=ClCH_3, F^-$) are then obtained from $\tilde{\rho}_R$ using the weight function, w_X associated with the same fragment. Thus

$$q_X = \int w_X(\mathbf{r})[\tilde{\rho}_R^\alpha(\mathbf{r}) + \tilde{\rho}_R^\beta(\mathbf{r})]d\mathbf{r}, \quad S_X = \int w_X(\mathbf{r})[\tilde{\rho}_R^\alpha(\mathbf{r}) - \tilde{\rho}_R^\beta(\mathbf{r})]d\mathbf{r}. \quad (19)$$

q_X and S_X are then used in a CDFT calculation to build the desired reactant state, as illustrated in Figure 5.

This diabatic procedure generalizes to any $AB+C \rightarrow A+BC$ reaction. Further, solving Eq. 10 typically gives better adiabatic reaction barrier heights than those obtained from the unconstrained ground state, as illustrated in Table I. Here, we consider the standard set of reaction barriers collected by Truhlar and coworkers [114] using both standard DFT and the CDFT- configuration interaction (CDFT-CI) energy of Eq. 10 using the diabatic prescription described above for reactant and product states. We see that the CDFT-CI results are typically significantly better than their unconstrained counterparts, particularly with less accurate functionals[110]. Only for B97-2, which already gives fairly accurate barrier heights, do the limitations of our diabatic prescription become apparent. The clear improvement in the CDFT-CI barrier heights can be traced to two sources. First, we note that a large fraction of the error in DFT barrier height predictions is known to arise from electron self-interaction error (SIE)[115, 116]. Because the constraints force the electrons to localize in every underlying diabatic state, the effects of SIE on the CDFT-CI results are mitigated[62, 64], improving the barrier heights. Second, by including a small CI within the calculation, CDFT-CI is able to include some of the static correlation that is missing in standard functionals[117], leading to a more stable description of bond breaking at the transition state.

TABLE I: Summary of the mean absolute error (MAE) of barrier heights. The numbers in parenthesis represent the total number of barrier heights in each data set. Numbers in black are CDFT-CI results. All energies are in kcal/mol.

	PBE	B3LYP	B97-2			
hydrogen transfer (36)						
MAE	9.7	3.8	4.6	3.0	3.6	4.0
heavy atom transfer (12)						
MAE	14.9	7.6	8.5	2.3	3.4	4.7
nucleophilic substitution (16)						
MAE	6.9	2.3	3.4	1.3	1.4	2.9
all (64)						
MAE	10.0	4.2	5.1	2.5	3.0	3.9

It is important to note that this same diabatic prescription can be used not only to obtain accurate results, but to physically interpret the results as well. For example, we can use the same CDFT-CI approach to treat bonding in LiF if we consider four diabatic states: Li^+F^- , $\text{Li}^\uparrow\text{F}^\downarrow$, $\text{Li}^\downarrow\text{F}^\uparrow$ and Li^-F^+ . One finds that this prescription gives a very accurate description of the adiabatic dissociation curve (See Figure 6) when compared to an accurate OD(2) calculation [118, 119]. However, the CDFT-CI calculation also allows us to break the adiabatic state down into contributions from the various ionic and covalent contributions. Thus we see that LiF is, indeed, primarily covalent beyond the capture radius of 5.4 Å, but that Li^+F^- becomes dominant as the bond becomes shorter.

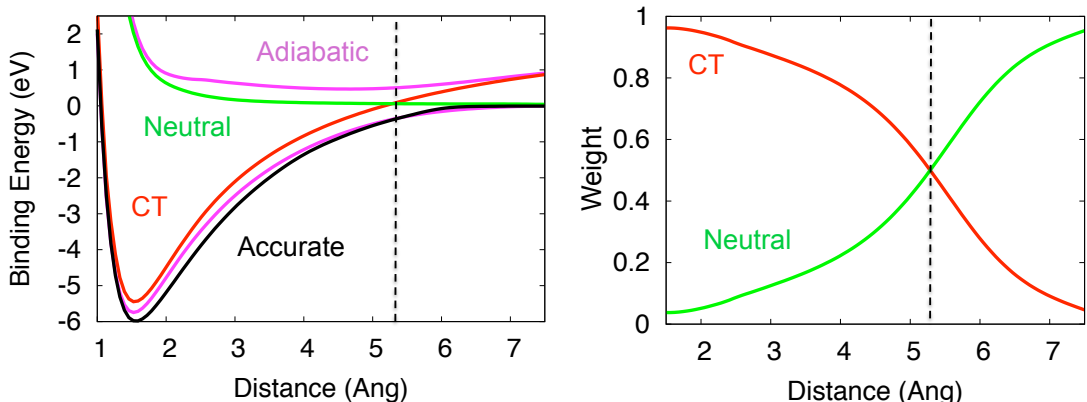


FIG. 6: (Left) Dissociation curves of LiF with various approximate methods. (Right) Weights of configurations in the CDFT-CI (B3LYP) ground state. The ground state rapidly switches from neutral to ionic at the capture radius for Li^+F^- ($R=5.4$ Å).

VI. CONCLUSIONS

In this review we have briefly highlighted the role diabatic states have in our qualitative understanding of chemistry as well as the fundamental equations that allow diabats to be used for quantitative prediction. The non-existence of strictly diabatic states leads to a variety of essentially diabatic states, each of which can be an appropriate description of chemistry under the right circumstances. For concreteness, we have focused here on the use of density constraints for the definition of diabats and have shown how the electronic energy, nuclear forces and diabatic coupling can be obtained in this particular representation. We

also illustrated how these diabatic states can be used for both the description of electron transfer chemistry and the prediction of reaction barrier heights.

Moving forward, we see an expanding role for diabatic states in the area of reaction dynamics - in particular excited state dynamics. Constructive strategies such as valence bond or constrained DFT techniques offer direct access to diabatic potential energy surfaces without recourse to the corresponding adiabats. Thus, energies, forces and molecular properties can easily be computed on-the-fly, facilitating MD simulation of large systems. Thus, in the case of electron transfer, one is already able to propagate trajectories on individual diabatic surfaces to sample the free energy landscape (See Figure 4) even when one of those states is not the ground state.

Future Issues

- Ideally, one would also like to create a less arbitrary construction of diabatic states that is still computationally inexpensive. At present, constrained DFT requires the identification of fragments and the (non-unique) choice of atomic populations. A prescription that automatically optimizes the fragment choice and the atomic populations based on energy minimization would clearly be preferable. In this area, the ideas of partition theory [120, 121] might provide a way forward.
- The results obtained so far indicate CDFT-CI gives accurate adiabatic ground state potential energy surfaces. The CI eigenequation (Eq. 10) also provides excited states. Under what circumstances are the excitation energies accurate?
- One would like to generate trajectories that allow quantum transitions between the diabatic electronic states. These simulations could employ, for example, surface hopping [122], multiple spawning [123] or generalized Langevin [124] techniques to describe the quantum transitions. Simulations of this type would be instrumental in directly predicting electron transfer kinetics from the dynamics.

Even without any further theoretical advances (see Future Issues) in our understanding of diabatic states, the existing technology is well-positioned to answer important chemical questions. The applications presented here have necessarily been by way of illustration and validation of the concepts involved. However, it should be clear that the same steps outlined above could be used in the description of ultrafast photoinduced ET in solution [125] or at interfaces [126] as well as in the description of reaction barriers in electrochemical[127],

photovoltaic [128] and photosynthetic [129] architectures. Thus, we see that while diabatic states have their historical origins in the qualitative description of chemistry, these same states promise to play an active role in the future of computational and theoretical chemistry.

Acknowledgments

This work was sponsored by an NSF-CAREER Award (CHE-0547877). TV gratefully acknowledges a Packard Fellowship and a Sloan Fellowship. QW acknowledges support from DOE-BES (DE-AC02-98CH10886).

Literature Cited

- [1] Köppel H, Domcke W, Cederbaum LS. 1984. Multimode molecular dynamics beyond the Born-Oppenheimer approximation. *Adv. Chem. Phys.* 57: 59-246.
- [2] Manthe U, Köppel H. 1990. Dynamics on potential energy surfaces with a conical intersection: Adiabatic, intermediate, and diabatic behavior. *J. Chem. Phys.* 93: 1658-1669.
- [3] Kim Y, Corchado JC, Villà J, Xing J, Truhlar DG. 2000. Multiconfiguration molecular mechanics algorithm for potential energy surfaces of chemical reactions. *J. Chem. Phys.* 112: 2718-2735.
- [4] Liyanage R, Gordon R, Field R. 1998. Diabatic analysis of the electronic states of hydrogen chloride. *J. Chem. Phys.* 109: 8374-8387.
- [5] Mueller J, Morton M, Curry S, Abbatt J, Butler L. 2000. Intersystem crossing and nonadiabatic product channels in the photodissociation of N₂O₄ at 193 nm. *J. Phys. Chem. A* 104: 4825-4832.
- [6] Ichino T, Gianola AJ, Lineberger WC, Stanton JF. 2006. Nonadiabatic effects in the photoelectron spectrum of the pyrazolide-*d*₃ anion: Three-state interactions in the pyrazolyl-*d*₃ radical. *J. Chem. Phys.* 125: 084312.
- [7] Gadéa FX, Péliissier M. 1990. Approximately diabatic states: A relation between effective Hamiltonian techniques and explicit cancellation of the derivative coupling. *J. Chem. Phys.* 93: 545-551.
- [8] Nakamura H. 1991. What are the basic mechanisms of electronic transitions in molecular dynamic processes?. *International Reviews in Physical Chemistry* 10: 123-188.
- [9] Woywod C, Stengle M, Domcke W, Flöthmann H, Schinke R. 1997. Photodissociation of ozone in the Chappuis band. I. Electronic structure calculations. *J. Chem. Phys.* 107: 7282-7295.
- [10] Müller U, Stock G. 1997. Surface-hopping modeling of photoinduced relaxation dynamics on coupled potential-energy surfaces. *J. Chem. Phys.* 107: 6230-45.
- [11] Butler LJ. 1998. Chemical reaction dynamics beyond the Born-Oppenheimer approximation. *Ann. Rev. Phys. Chem.* 49: 125-171.

- [12] Cohen JM, Micha DA. 1992. Electronically diabatic atom–atom collisions: A self-consistent eikonal approximation. *J. Chem. Phys.* 97: 1038-1052.
- [13] Tully JC. 2000. Chemical dynamics at metal surfaces. *Ann. Rev. Phys. Chem.* 51: 153-178.
- [14] Mahapatra S, Koppel H, Cederbaum LS. 2001. Reactive scattering dynamics on conically intersecting potential energy surfaces: The H + H₂ exchange reaction. *J. Phys. Chem. A* 105: 2321-2329.
- [15] Pauling L1960. *The Nature of the Chemical Bond* (Cornell University Press, Ithaca, NY, 1960), 3rd ed.
- [16] Warshel A, Weiss RM. 1980. An empirical valence bond approach for comparing reactions in solutions and in enzymes. *J. Am. Chem. Soc.* 102: 6218-6226.
- [17] Åqvist J, Warshel A. 1993. Simulation of enzyme reactions using valence-bond force fields and other hybrid quantum-classical approaches. *Chem. Rev.* 93: 2523-2544.
- [18] Sidis V. 1992. Diabatic potential-energy surfaces for charge-transfer processes. *Adv. Chem. Phys.* 82: 73-134.
- [19] Marcus RA. 1985. Electron transfers in chemistry and biology. *Biochim. Biophys. Acta* 811: 265-322.
- [20] Timoneda JJI, Hynes JT. 1991. Nonequilibrium free energy surfaces for hydrogen-bonded proton-transfer complexes in solution. *J. Chem. Phys.* 95: 10431-10442.
- [21] Hammes-Schiffer S, Tully JC. 1994. Proton transfer in solution: Molecular dynamics with quantum transitions. *J. Chem. Phys.* 101: 4657-4667.
- [22] Kuznetsov AM, Ulstrup J. 1999. Proton and hydrogen atom tunnelling in hydrolytic and redox enzyme catalysis. *Can. J. Chem.* 77: 1085-1096.
- [23] Mead CA, Truhlar DG. 1982. Conditions for the definition of a strictly diabatic electronic basis for molecular-systems. *J. Chem. Phys.* 77: 6090.
- [24] Baer M. 1975. Adiabatic and diabatic representations for atom-molecule collisions: Treatment of the collinear arrangement. *Chem. Phys. Lett.* 35: 112-118.
- [25] Baer M. 1980. Electronic non-adiabatic transitions - derivation of the general adiabatic-diabatic transformation matrix. *Mol. Phys.* 40: 1011-1013.
- [26] Baer M, Englman R. 1992. A study of the diabatic electronic representation within the Born-Oppenheimer approximation. *Mol. Phys.* 75: 293-303.
- [27] Pacher T, Cederbaum LS, Köppel H. 1993. Adiabatic and quasidiabatic states in a gauge

- theoretical framework. *Adv. Chem. Phys.* 84: 293-391.
- [28] Pacher T, Cederbaum LS, Köppel H. 1988. Approximately diabatic states from block diagonalization of the electronic Hamiltonian. *J. Chem. Phys.* 89: 7367-7381.
- [29] Pacher T, Köppel H, Cederbaum LS. 1991. Quasidiabatic states from ab initio calculations by block diagonalization of the electronic Hamiltonian - use of frozen orbitals. *J. Chem. Phys.* 95: 6668-6680.
- [30] Pacher T, Mead CA, Cederbaum LS, Köppel H. 1989. Gauge theory and quasidiabatic states in molecular physics. *J. Chem. Phys.* 91: 7057-7062.
- [31] Ruedenberg K, Atchity GJ. 1993. A quantum-chemical determination of diabatic states. *J. Chem. Phys.* 99: 3799-3803.
- [32] Atchity GJ, Ruedenberg K. 1997. Determination of diabatic states through enforcement of configurational uniformity. *Theor. Chem. Acc.* 97: 47-58.
- [33] Thiel A, Köppel H. 1999. Proposal and numerical test of a simple diabatization scheme. *J. Chem. Phys.* 110: 9371-9383.
- [34] Köppel H, Gronki J, Mahapatra S. 2001. Construction scheme for regularized diabatic states. *J. Chem. Phys.* 115: 2377-2388.
- [35] Nakamura H, Truhlar DG. 2001. The direct calculation of diabatic states based on configurational uniformity. *J. Chem. Phys.* 115: 10353-10372.
- [36] Nakamura H, Truhlar DG. 2002. Direct diabatization of electronic states by the fourfold way. II. Dynamical correlation and rearrangement processes. *J. Chem. Phys.* 117: 5576-5593.
- [37] Mulliken R. 1952. Molecular compounds and their spectra. II. *J. Am. Chem. Soc.* 74: 811-824.
- [38] Hush N. 1967. Intervalence-transfer absorption. Part 2. Theoretical considerations and spectroscopic data. *Prog. Inorg. Chem.* 8: 391-444.
- [39] Cave RJ, Newton MD. 1996. Generalization of the Mulliken-Hush treatment for the calculation of electron transfer matrix elements. *Chem. Phys. Lett.* 249: 15-19.
- [40] Cave RJ, Newton MD. 1997. Calculation of electronic coupling matrix elements for ground and excited state electron transfer reactions: Comparison of the generalized Mulliken-Hush and block diagonalization methods. *J. Chem. Phys.* 106: 9213-9226.
- [41] Werner HJ, Meyer W. 1981. MCSCF study of the avoided curve crossing of the two lowest $^1\sigma_+$ states of LiF. *J. Chem. Phys.* 74: 5802-5807.
- [42] Boys SF. 1960. Construction of some molecular orbitals to be approximately invariant for

- changes from one molecule to another. *Rev. Mod. Phys* 32: 296-299.
- [43] Subotnik JE, Yeganeh S, Cave RJ, Ratner MA. 2008. Constructing diabatic states from adiabatic states: Extending generalized Mulliken Hush to multiple charge centers with Boys localization. *J. Chem. Phys.* 129: 244101.
- [44] Pauling, L. 1960. *The Nature of the Chemical Bond*. Ithaca, NY: Cornell University Press, 3rd ed.
- [45] Truhlar DG. 2007. Valence bond theory for chemical dynamics. *J. Comp. Chem.* 28: 73-86.
- [46] Song LC, Gao JL. 2008. On the construction of diabatic and adiabatic potential energy surfaces based on ab initio valence bond theory. *J. Phys. Chem. A* 112: 12925-12935.
- [47] Kim HJ, Hynes JT. 1992. A theoretical model for S_N1 ionic dissociation in solution. 1. Activation free energetics and transition state structure. *J. Am. Chem. Soc.* 114: 10508-10528.
- [48] Soudackov A, Hammes-Schiffer S. 2000. Derivation of rate expressions for nonadiabatic proton-coupled electron transfer reactions in solution. *J. Chem. Phys.* 113: 2385-2396.
- [49] Mo YR, Gao JL. 2000. An ab initio molecular orbital-valence bond (MOVB) method for simulating chemical reactions in solution. *J. Phys. Chem. A* 104: 3012-3020.
- [50] Gerratt J, Cooper DL, Karadakov PB, Raimondi M. 1997. Modern valence bond theory. *Chem. Soc. Rev.* 26: 87-100.
- [51] Wesolowski TA, Warshel A. 1993. Frozen density-functional approach for ab initio calculations of solvated molecules. *J. Phys. Chem.* 97: 8050-8053.
- [52] Olsson MHM, Hong GY, Warshel A. 2003. Frozen density functional free energy simulations of redox proteins: Computational studies of the reduction potential of plastocyanin. *J. Am. Chem. Soc.* 2003: 5025-5039.
- [53] Dederichs PH, Blügel S, Zeller R, Akai H. 1984. Ground states of constrained systems: Application to Cerium impurities. *Phys. Rev. Lett.* 53: 2512-2515.
- [54] Okamoto K *et al.*. 2005. Drastic difference in lifetimes of the charge-separated state of the formanilide-anthraquinone dyad versus the ferrocene-formanilide-anthraquinone triad and their photoelectrochemical properties of the composite films with fullerene clusters. *J. Phys. Chem. A* 109: 4662-4670.
- [55] Wu Q, Van Voorhis T. 2006. Direct calculation of electron transfer parameters through constrained density functional theory. *J. Phys. Chem. A* 110: 9212-9218.

- [56] Mulliken RS. 1955. Electronic populations analysis on LCAO-MO molecular wave functions. *J. Chem. Phys.* 23: 1833-1840.
- [57] Löwdin PO. 1950. On the non-orthogonality problem connected with the use of atomic wave functions in the theory of molecules and crystals. *J. Chem. Phys.* 18: 365-375.
- [58] Bader RFW. 1985. Atoms in molecules. *Accounts Chem. Res.* 18: 9-15.
- [59] Becke AD. 1988. A multicenter numerical integration scheme for polyatomic molecules. *J. Chem. Phys.* 88: 2547-2553.
- [60] Hirshfeld FL. 1977. Bonded-atom fragments for describing molecular charge densities. *Theo. Chem. Acc.* 44: 129-138.
- [61] Wu Q, Van Voorhis T. 2005. A direct optimization method to study constrained systems within density functional theory. *Phys. Rev. A* 72: 024502.
- [62] Wu Q, Van Voorhis T. 2006. Constrained density functional theory and its application in long range electron transfer. *J. Chem. Theo. Comp.* 2: 765-774.
- [63] Behler J, Delley B, Lorenz S, Reuter K, Scheffler M. 2005. Dissociation of O₂ at Al(111): The role of spin selection rules. *Phys. Rev. Lett.* 94: 036104.
- [64] Rudra I, Wu Q, Van Voorhis T. 2006. Accurate magnetic exchange couplings in transition metal complexes from constrained density functional theory. *J. Chem. Phys.* 24: 024103.
- [65] Rudra I, Wu Q, Van Voorhis T. 2007. Predicting exchange coupling constants in frustrated molecular magnets using density functional theory. *Inorg. Chem.* 46: 10539-10548.
- [66] Behler J, Delley B, Reuter K, Scheffler M. 2007. Nonadiabatic potential-energy surfaces by constrained density-functional theory. *Phys. Rev. B* 75.
- [67] High Performance Computational Chemistry Group. 2004. *NWChem, A Computational Chemistry Package for Parallel Computers, Version 5.0*. Pacific Northwest National Laboratory, Richland, Washington.
- [68] Shao Y *et al.*. 2006. Advances in methods and algorithms in a modern quantum chemistry program package. *Phys. Chem. Chem. Phys.* 8: 3172-3191.
- [69] Becke AD. 1993. Density-functional thermochemistry .3. the role of exact exchange. *J. Chem. Phys.* 98: 5648-5652.
- [70] Klamt A, Schuurmann G. 1993. COSMO - a new approach to dielectric screening in solvents with explicit expressions for the screening energy and its gradient. *J. Chem. Soc. Perk. T. 2* 5: 799-805.

- [71] Rehm D, Weller A. 1970. Kinetics of fluorescence quenching by electron transfer and H-atom transfer. *Israel J. Chem.* 8: 259-271.
- [72] Siders P, Cave RJ, Marcus RA. 1984. Model for orientation effects in electron transfer reactions. *J. Chem. Phys.* 81: 5613-5624.
- [73] Daizadeh I, Medvedev ES, Stuchebrukhov AA. 1997. Effect of protein dynamics on biological electron transfer. *Proc. Nat. Acad. Sci.* 94: 3703-3708.
- [74] Note that the many theories besides DFT - including many body perturbation theory, coupled cluster theory and reduced density matrix theory - also avoid explicit computation of the wavefunction in one form or another, making the computation of V_{ij} a challenge in these cases as well.
- [75] Wu Q, Van Voorhis T. 2006. Extracting electron transfer coupling elements from constrained density functional theory. *J. Chem. Phys.* 125: 164105.
- [76] Watchers AJH. 1970. Gaussian basis set for molecular wavefunctions containing third-row atoms. *J. Chem. Phys.* 52: 1033-1036.
- [77] Barbara PF, Meyer TJ, Ratner MA. 1996. Contemporary issues in electron transfer research. *J. Phys. Chem.* 100: 13148-13168.
- [78] Barbara PF, Jarzaba W. 1990. Ultrafast photochemical intramolecular charge transfer and excited state solvation. *Adv. Photochem.* 15: 1-68.
- [79] Marcus RA. 1964. Chemical and electrochemical electron-transfer theory. *Ann. Rev. Phys. Chem.* 15: 155-196.
- [80] Kestner NR, Logan J, Jortner J. 1974. Thermal electron transfer reactions in polar solvents. *J. Phys. Chem.* 78: 2148-2166.
- [81] Small DW, Matyushov DV, Voth GA. 2003. The theory of electron transfer reactions: What may be missing?. *J. Am. Chem. Soc.* 125: 7470-7478.
- [82] Hush NS. 1961. Adiabatic theory of outer sphere electron-transfer reactions in solution. *Trans. Farad. Soc.* 57: 557-580.
- [83] Jortner J. 1976. Temperature dependent activation energy for electron transfer between biological molecules. *J. Chem. Phys.* 64: 4860-4867.
- [84] Sit PHL, Cococcioni M, Marzari N. 2006. Realistic quantitative descriptions of electron transfer reactions: Diabatic free-energy surfaces from first-principles molecular dynamics. *Phys. Rev. Lett.* 97: 028303.

- [85] Marcus RA. 1956. On the theory of oxidation-reduction reactions involving electron transfer. I.. *J. Chem. Phys.* 24: 966-978.
- [86] Carter EA, Hynes JT. 1991. Solvation dynamics for an ion pair in a polar solvent: Time-dependent fluorescence and photochemical charge transfer. *J. Chem. Phys.* 94: 5961-5979.
- [87] Hwang JK, Warshel A. 1987. Microscopic examination of free-energy relationships for electron-transfer in polar solvents. *J. Am. Chem. Soc.* 109: 715-720.
- [88] Tachiya M. 1989. Relation between the electron-transfer rate and the free energy change of reaction. *J. Phys. Chem.* 93: 7050-7052.
- [89] Subotnik JE, Cave RJ, Steele RP, Shenoi N. 2009. The initial and final states of electron and energy transfer processes: Diabatization as motivated by system-solvent interactions. *J. Chem. Phys.* 130.
- [90] Onsager L. 1936. Electric moments of molecules in liquids. *J. Am. Chem. Soc.* 58: 1486-1493.
- [91] Rinaldi D, Ruiz-Lopez MF, Rivail JL. 1983. Ab initio SCF calculations on electrostatically solvated molecules using a deformable three axes ellipsoidal cavity. *J. Chem. Phys.* 78: 834-838.
- [92] Barone V, Cossi M. 1998. Quantum calculation of molecular energies and energy gradients in solution by a conductor solvent model. *J. Phys. Chem. A* 102: 1995-2001.
- [93] Cramer CJ, Truhlar DG. 1999. Implicit solvation models: Equilibria, structure, spectra, and dynamics. *Chem. Rev.* 99: 2161-2200.
- [94] Hsu CP, Song X, Marcus RA. 1997. Time-dependent Stokes shift and its calculation from solvent dielectric dispersion data. *J. Phys. Chem. B* 101: 2546-2551.
- [95] Cramer CJ, Truhlar DG. 1992. An SCF solvation model for the hydrophobic effect and absolute free energies of aqueous solvation. *Science* 256: 213-217.
- [96] Mennucci B, Tomasi J. 1997. Continuum solvation models: A new approach to the problem of solute's charge distribution and cavity boundaries. *J. Chem. Phys.* 106: 5151-5158.
- [97] Cossi M, Barone V. 2000. Solvent effect on vertical electronic transitions by the polarizable continuum model. *J. Chem. Phys.* 112: 2427-2435.
- [98] Warshel A. 1982. Dynamics of reactions in polar solvents - semi-classical trajectory studies of electron-transfer and proton-transfer reactions. *J. Phys. Chem.* 86: 2218-2224.
- [99] Warshel A, Hwang JK. 1986. Simulation of the dynamics of electron-transfer reactions in polar solvents - semiclassical trajectories and dispersed polaron approaches. *J. Chem. Phys.*

- 84: 4938-4957.
- [100] Zichi DA, Ciccotti G, Hynes JT, Ferrario M. 1989. Molecular dynamics simulation of electron-transfer reactions in solution. *J. Phys. Chem.* 93: 6261-6265.
- [101] King G, Warshel A. 1990. Investigation of the free-energy functions for electron transfer reactions. *J. Chem. Phys.* 93: 8682-8692.
- [102] Kuharski RA *et al.*. 1988. Molecular model for aqueous ferrous-ferric electron transfer. *J. Chem. Phys.* 89: 3248-3257.
- [103] Bader RS, Kuharski RA, Chandler D. 1990. Role of nuclear tunneling in aqueous ferrous-ferric electron transfer. *J. Chem. Phys.* 93: 230-236.
- [104] Bader RS, Chandler D. 1989. Computer simulation of photochemically induced electron-transfer. *Chem. Phys. Lett.* 157: 501-504.
- [105] Blumberger J, Sprik M. 2005. Ab initio molecular dynamics simulation of the aqueous $\text{Ru}^{2+}/\text{Ru}^{3+}$ redox reaction: The Marcus perspective. *J. Phys. Chem. B* 109: 6793-6804.
- [106] Tateyama Y, Blumberger J, Sprik M, Tavernelli I. 2005. Density-functional molecular-dynamics study of the redox reactions of two anionic, aqueous transition-metal complexes. *J. Chem. Phys.* 122.
- [107] Blumberger J, Sprik M. 2006. Quantum versus classical electron transfer energy as reaction coordinate for the aqueous $\text{Ru}^{2+}/\text{Ru}^{3+}$ redox reaction. *Theo. Chem. Acc.* 115: 113-126.
- [108] VandeVondele J, Lynden-Bell R, Meijer EJ, Sprik M. 2006. Density functional theory study of tetrathiafulvalene and thianthrene in acetonitrile: Structure, dynamics, and redox properties. *J. Phys. Chem. B* 110: 3614-3623.
- [109] VandeVondele J, Ayala R, Sulpizi M, Sprik M. 2007. Redox free energies and one-electron energy levels in density functional theory based ab initio molecular dynamics. *J. Electroanal. Chem.* 607: 113-120.
- [110] Kowalczyk T, Wang LP, Van Voorhis T. 2009. In preparation. (2009).
- [111] Sulpizi M, Raugei S, VandeVondele J, Carloni P, Sprik M. 2007. Calculation of redox properties: Understanding short- and long-range effects in rubredoxin. *J. Phys. Chem. B* 111: 3969-3976.
- [112] Mo YR, Gao JL. 2000. Ab initio QM/MM simulations with a molecular orbital-valence bond (MOVB) method: application to an $\text{S}_\text{N}2$ reaction in water. *J. Comp. Chem.* 21: 1458-1469.
- [113] Wu Q, Cheng CL, Van Voorhis T. 2007. Configuration interaction based on constrained

- density functional theory. *J. Chem. Phys.* 127: 164119.
- [114] Zhao Y, Gonzalez-Garcia N, Truhlar DG. 2005. Benchmark database of barrier heights for heavy atom transfer, nucleophilic substitution, association, and unimolecular reactions and its use to test theoretical methods. *J. Phys. Chem. A* 109: 2012-2018.
- [115] Vydrov OA, Scuseria GE. 2006. Assessment of a long-range corrected hybrid functional. *J. Chem. Phys.* 125: 234109.
- [116] Janesko BG, Scuseria GE. 2008. Hartree–Fock orbitals significantly improve the reaction barrier heights predicted by semilocal density functionals. *J. Chem. Phys.* 128: 244112.
- [117] Cremer D. 2001. Density functional theory: coverage of dynamic and non-dynamic electron correlation effects. *Mol. Phys.* 99: 1899-1940.
- [118] Sherrill CD, Krylov AI, Byrd EFC, Head-Gordon M. 1998. Energies and analytic gradients for a coupled-cluster doubles model using variational Brueckner orbitals: Application to symmetry breaking in O_4^+ . *J. Chem. Phys.* 109: 4171.
- [119] Gwaltney SR, Head-Gordon M. 2000. A second-order correction to singles and doubles coupled-cluster methods based on a perturbative expansion of a similarity transformed Hamiltonian. *Chem. Phys. Lett.* 323: 21-28.
- [120] Cohen MH, Wasserman A. 2007. On the foundations of chemical reactivity theory. *J. Phys. Chem. A* 111: 2229-2242.
- [121] Elliott P, Cohen MH, Wasserman A, Burke K. 2009. Density functional partition theory with fractional occupations. *J. Chem. Theo. Comp.* 5: 827-833.
- [122] Tully JC. 1990. Molecular dynamics with electronic transitions. *J. Chem. Phys.* 93: 1061-1071.
- [123] Ben-Nun M, Quenneville J, Martinez TJ. 2000. Ab initio multiple spawning: Photochemistry from first principles quantum molecular dynamics. *J. Phys. Chem. A* 104: 5161-5175.
- [124] Song X, Wang HB, Van Voorhis T. 2008. A Langevin equation approach to electron transfer reactions in the diabatic basis. *J. Chem. Phys.* 129: 144502.
- [125] Maroncelli M, MacInnis J, Fleming GR. 1989. Polar-solvent dynamics and electron transfer reactions. *Science* 243: 1674-1681.
- [126] Asbury JB, Hao E, Wang Y, Ghosh HN, Lian T. 2001. Ultrafast electron transfer dynamics from molecular adsorbates to semiconductor nanocrystalline thin films. *J. Phys. Chem. B* 105: 4545-4557.

- [127] Grätzel M. 2001. Photoelectrochemical cells. *Nature* 414: 338-344.
- [128] Peumans P, Yakimov A, Forrest SR. 2003. Small molecular weight organic thin-film photodetectors and solar cells. *J. Appl. Phys.* 93: 3693-3723.
- [129] Ferreira KN, Iverson TM, Maghlaoui K, Barber J, Iwata S. 2004. Architecture of the photosynthetic oxygen-evolving center. *Science* 303: 1831-1838.

Brief Annotations

- Ref. 1** Presents an extensive introduction to the use of diabatic states in modeling vibronic dynamics.
- Ref 15** An enduring classic. Highlights the important contributions of the valence bond picture of chemical binding.
- Ref. 16** An article many years ahead of its time that introduces the empirical VB concept.
- Ref. 19** A broad review of the relevance of ET in chemistry and biology.
- Ref. 45** A unique perspective on the role of VB in chemistry.
- Ref. 55** Presents the connection between CDFT and ET.
- Ref. 75** Introduces the definition of the diabatic coupling in CDFT.
- Ref. 77** An approachable introduction to electron transfer in chemical physics.

FIG. 1: NaCl dissociation in the diabatic and adiabatic representations. The ionic (green) and covalent (blue) diabatic states maintain the same character across the potential energy surface, while the adiabatic states (black) change.

FIG. 2: Obtaining the D^+A^- state of FAAQ. a) One chooses which atoms belong to the acceptor. The atomic partition operator then divides space between the fragments, as illustrated by the dividing surface. b) Apply a constraint potential. Changing the Lagrange multiplier changes the depth of the potential and controls the number of charges on the acceptor. c) A ground state calculation in the presence of the optimal potential results in exactly one excess electron (red) on the acceptor and one excess hole (blue) on the donor.

FIG. 3: A) In solution, the electron transfer reaction coordinate is dominated by solvent reorganization. The free energy landscape can be characterized by the driving force (ΔG), measuring the energy released, and reorganization energy (λ), measuring the structural relaxation energy. B) If $\Delta G < \lambda$ the reaction is in the normal regime and the rate increases with ΔG , but C) if $\Delta G > \lambda$ the reaction is inverted and the rate decreases with increasing ΔG

FIG. 4: Sampling the ET energy landscape with explicit solvent. a) One first computes several long MD trajectories, with the solute in either the neutral (pictured) or CT state. A movie of one such trajectory is available in the supporting material. b) One monitors the energy of each diabatic as a function of time and collects statistics on the energy gap ($\Delta E = E_{CT} - E_N$) from the neutral (c) and CT (d) trajectories. Here, the histograms show accumulated data, while the lines are a maximum likelihood fit. e) Finally, the free energy, G of each state is computed from the log of the probability computed in parts c) and d). All energies are in eV.

FIG. 5: Constructing reactant and product diabatic states for $F^- + CH_3Cl \leftrightarrow FCH_3 + Cl^-$. a) The atoms are divided according to the reactants and products b) DFT calculations are performed on the isolated fragments c) The fragment densities are added together d) The apparent charge (N) and spin (S) for each fragment are determined by integrating the population weight function $w_i(\mathbf{r})$ against the summed densities e) Constrained DFT calculations are performed with the computed N+S constraints to arrive at the reactant and product diabats.

FIG. 6: (Left) Dissociation curves of LiF with various approximate methods. (Right) Weights of configurations in the CDFT-CI (B3LYP) ground state. The ground state rapidly switches from neutral to ionic at the capture radius for Li^+F^- ($R=5.4 \text{ \AA}$).

TABLE I: Summary of the mean absolute error (MAE) of barrier heights. The numbers in parenthesis represent the total number of barrier heights in each data set. Numbers in black are CDFT-CI results. All energies are in kcal/mol.

	PBE	B3LYP	B97-2			
hydrogen transfer (36)						
MAE	9.7	3.8	4.6	3.0	3.6	4.0
heavy atom transfer (12)						
MAE	14.9	7.6	8.5	2.3	3.4	4.7
nucleophilic substitution (16)						
MAE	6.9	2.3	3.4	1.3	1.4	2.9
all (64)						
MAE	10.0	4.2	5.1	2.5	3.0	3.9

